

Shock Initiation of the Triaminotrinitrobenzene-Based Explosive JBO-9021 Measured with a Photon Doppler Velocimeter

Tao Zhang,^[a] Ji-bo Zhao,^[a] Zhi-peng Gao,^[a] Xing Wu,^[b] Hong-liang He,^[a] and Yan Gu^{*[a]}

Abstract: Triaminotrinitrobenzene (TATB) is an important insensitive high explosive because of its low shock sensitivity and high energy. The evolution of shock into the detonation of TATB requires academic attention and research. A multi-points laser interferometer termed a photon Doppler velocimeter and a rotating mirror streak camera were used to study the shock initiation of detonation in a pressed solid explosive formulation, JBO-9021, which contained 85 wt.% TATB, 10 wt.% HMX and 5 wt.% Kel-F binder. In conventional experiments, the test explosive was assembled by using several columniform explosives with different external diameters. A new device was designed to solve complex problems. This device comprised a wedge-shaped explosive sample and a transparent window, and by using this device, the particle-velocity histories of eight

shock positions and the shockwave velocity could be obtained. A series of shock-initiation experiments on high explosive JBO-9021 was performed, and the explosive samples were initiated at different intensity input shocks by an explosive-driven attenuator. The photon Doppler velocimeter was used to detail the growth from an input shock to detonation, and the increase in particle velocity in unreacted JBO-9021 was also obtained in low-intensity shock-initiation experiments. The shock velocity was measured with a rotating mirror streak camera in one experiment. Hugoniot data for JBO-9021 in the form of a shock velocity versus a particle velocity and the initial shock pressure versus a distance-to-detonation relationship (Pop-plot) were obtained. Based on the experimental results, the shock-sensitivity characteristic of JBO-9021 was described.

Keywords: TATB · Photon Doppler velocimeter · Shock initiation · Pop-plot · Hugoniot

1 Introduction

The shock initiation of triaminotrinitrobenzene (TATB) explosives is of wide interest because of general safety concerns. JBO-9021, which is a mixed explosive with a high TATB content, has a high detonation energy and is poorly shock sensitive. Insight into the shock-initiation characteristics of JBO-9021 is of vital significance in explosive design and safety analysis. In the experimental study of shock initiation, piezoresistive pressure gauges are usually used to measure pressure histories during shock evolution into detonation. For instance, the shock sensitivity of LX-10 (HMX/Viton/95/5) was tested by Vandersall et al [1]. A 101-mm diameter propellant-driven gas gun at Lawrence Livermore National Laboratory (LLNL) was used to initiate the explosive sample that comprised manganin piezoresistive pressure gauges, and the pressure histories of shock into detonation of LX-10 were measured. Because of the low breakdown strength of manganin, the duration of the gauge-measuring pressure histories would be short for a strong release wave. The shockwave propagation will be disturbed by the manganin piezoresistive pressure gauges that are installed in the sample. These disadvantages could be avoided by using an in-situ laser interferometer. The laser interferometer is an optical-based system that uses Dop-

pler interferometry techniques to measure the complete time history of the surface motion. Two important features make the laser interferometer indispensable for shock-wave experiments. It can measure the Doppler shift of light that is scattered off diffuse surfaces; and its sensitivity is adjustable over a wide range. The laser interferometer is based on a simple physics principle [2] in which temporally coherent laser light illuminates a target surface for velocity measurement. Target motion produces a Doppler shift of the scattered light that causes the interference fringes to shift. A record of this shift yields a velocity history because it is proportional to the target velocity. The velocity interferometer system for any reflector (VISAR) was developed by Barker in 1972, and has been hailed a milestone in laser-interferometer history [2]. Since then, it has become a common tool that is used in experiments where high surface ve-

[a] T. Zhang, J.-b. Zhao, Z.-p. Gao, H.-l. He, Y. Gu
*National Key Laboratory of Shock Wave and Detonation Physics,
Institute of Fluid Physics, China Academy of Engineering Physics,
Mianyang, Sichuan, 621900, China*
*e-mail: guyan@caep.cn

[b] X. Wu
Institute of System Engineering, China Academy of Engineering Physics, Mianyang 621900, China

locities must be measured, and the shock sensitivity of many different types of explosives has been studied by multi-point laser interferometry [3–7]. The use of interface velocimetry to investigate the shock-initiation character and reaction zones of TATB-based explosives has been a continued effort of Wackerle's group for several years [3]. A dual Fabry-Perot velocimeter was used to measure the interface particle-velocity histories of thin PBX 9502 explosive disks with strong shock. A rounded character was resolved in the initial portion of the velocity histories. A shock-change analysis shows that this observation requires that reaction rates immediately behind the shock front be small relative to the subsequent rates in the evolution to detonation. Explosive initiation and energy release have been studied in a sample geometry that was designed to minimize stochastic behavior in shock-loading experiments by velocity interferometry diagnostics (single-point VISAR and a line-imaging optically recording velocity interferometer system) by Trott et al [4]. Initiation and reaction growth in pure and sensitized nitromethane result in wave profiles that are similar to those observed with heterogeneous explosives. In these experiments, the particle velocities at several distances from the impact surface are measured. Compared with manganin gauging, the laser-interferometer technique has several advantages. First, the sample is not required to be pressed into many thin pieces, so the difficulty of pressing the explosive is reduced. In addition, the use of a laser interferometer to observe interface velocity histories as waves that are propagated from the explosive into appropriate window materials does not require sample contact, so the accuracy of the experiment is improved.

A high-speed multi-point laser interferometer, termed the photon Doppler velocimeter, and a rotating mirror streak camera were used to investigate the evolution of shock into JBO-9021 explosive detonation at several shock input pressures experimentally, and the explosive sample was initiated by an explosive-driven shockwave generator. Interface particle-velocity histories at several distances from the impact surface were measured using the high-spatial-resolution capabilities of a photon Doppler velocimeter. Multiple fiber optics of the photon Doppler velocimeter used to send and receive Doppler information from a target were fixed at a specified distance above the sample. Shock velocities were measured with a streak camera. Run distances and times to detonation as a function of initial pressure were presented and the ignition and growth reactive-flow model were used to simulate the shock initiation of JBO-9021.

2 Experimental Section

The overall configuration for the initiation experimental apparatus is shown in Figure 1. The device consisted of a detonator, an explosive plane wave lens, a booster explosive, a tungsten-alloy attenuator plate, a lithium-fluoride (LiF) sin-

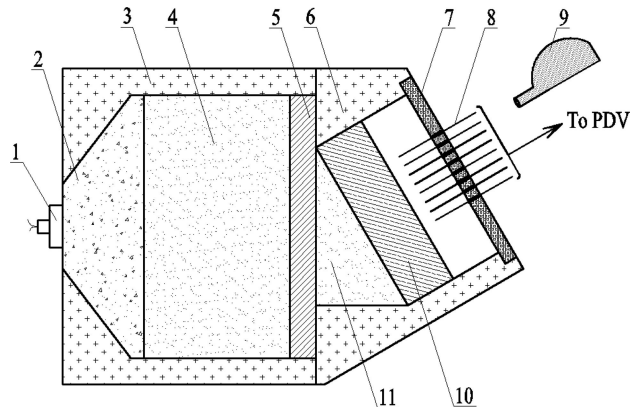


Figure 1. Schematic of the shock initiation experimental apparatus.
1- Detonator, 2- Explosive plane wave lens, 3- Base, 4- Booster explosive, 5- Tungsten alloy attenuator, 6- Specimen cell, 7- Fiber probe fixture, 8- Photon Doppler velocimeter fiber probe, 9- Rotating mirror streak camera, 10- LiF single crystal window, 11- Explosive specimen:

gle-crystal window, a fiber probe fixture, fiber probes, a rotating mirror streak camera and an explosive sample. The shock-compression experiments used an explosive-plane wave lens and booster explosive to provide well-controlled, reasonably planar and very reproducible input shock conditions, which were attenuated by the tungsten-alloy attenuator. When the plane shockwave propagates into the JBO-9021 explosive sample, the initiation of the explosive sample commenced. The shockwave that was provided by the explosive-plane wave lens has a plane area with a diameter of approximately 80 mm, and it fulfills the needs of the experiments. The intensity of the initial shock pressure could be adjusted by changing the thickness of the tungsten-alloy attenuator. The diameters of the explosive plane wave lens, booster explosive and tungsten-alloy attenuator plate were 100 mm. The JBO-9021 explosive samples were pressed into rectangular wedges, with an angle of 30°, a height of 35 mm and a width of 50 mm and details are shown in Figure 2(a). A transparent LiF plate (9-mm-thick) with a reflective coating (a 1-μm-thick buffer layer of aluminum) on the distal side (with respect to shock propagation direction) served as a window for velocity interferometry, and details are provided in Figure 2(b). The single-crystal LiF windows used mostly in this study have a slightly higher shock impedance than JBO-9021, so a slight shockwave is reflected back into the reacting explosive. The crystal has linear refractive index-density relationships, and is well-calibrated for the simple and accurate conversion of an apparent interface to a true value. This LiF window is attached to the explosive sample with the reflective coating side adhered to the sample using a very thin adhesive layer. The velocity interferometry diagnostics used in this study included a dual-delay-leg and photon Doppler velocimeter instrumentation for eight-point measurements that were capable of probing mesoscopic-scale phenomena. Fiber

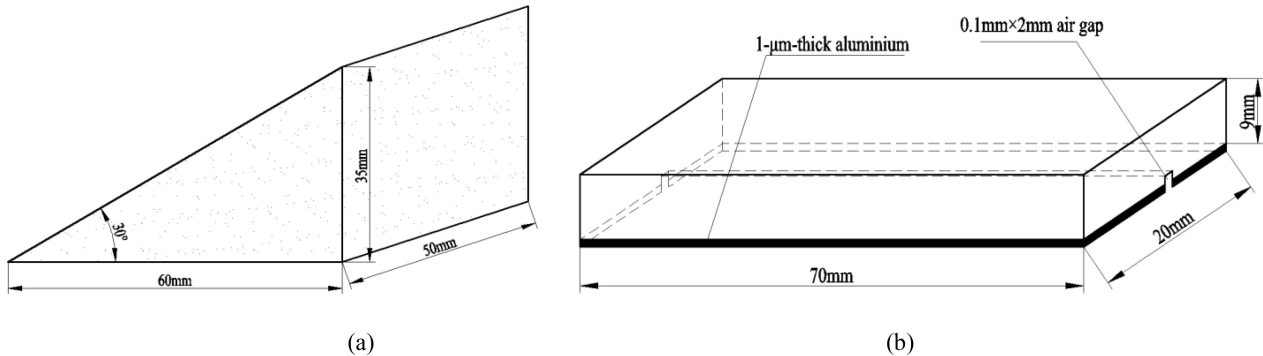


Figure 2. Schematic drawing of (a) explosive specimen and (b) LiF single crystal window.

probes were used to deliver the photon Doppler velocimeter source illumination to the target fixture and to collect the reflected light, and they were glued to the fixture using epoxy adhesive. The fiber probes were spaced 2 mm apart and the distance between the explosive sample and the fiber probe is 5 mm. As the shock travels through the sample and into the window, a particle-velocity history is generated, which causes a Doppler shift in the laser light that is analyzed by photon Doppler velocimeter diagnostics. If the shock Hugoniot is known for window and sample materials, the shock pressure of the sample can be derived from the particle velocity.

A streak camera was used at the interface of the sample and window, and it provided a measurement of the shock-wave propagation. The shockwave or detonation-wave velocity could be obtained independently from time of arrival at the different positions with a streak camera. The lighting method used to observe the shockwave or detonation wave on a single wedge-shaped test explosive charge is shown in Figure 2(b). A 0.1-mm-high, 2-mm-wide groove was scribed on the LiF single-crystal window surface and covered to the surface of the explosives, which created an air gap. When the detonation wave strikes this gap, the shocked air in the gap flashes. The advantage of this method is that no external light source is required and this method is suitable for use with JBO-9021 because the detonation wave in JBO-9021 was sufficiently strong to produce adequate light for recording by a rotating mirror streak camera. The initial shock pressure in the explosive samples was determined with an impedance-match technique, using the measured interface velocity and the measured shock velocity.

A photograph of the overall configuration of the initiation experiment is shown in Figure 3. Eight fiber probes were inserted into the fixture from 8 to 22 mm in 2-mm increments. To investigate the particle velocity after the turnover to detonation, a 100-mm diameter and 50-mm high JBO-9021 explosive disk were placed under the tungsten-alloy attenuator plate. By doing so, the input shock could start the initiation process of the explosive sample. The initial density of the JBO-9021 explosive was 1.905 g/cm³.

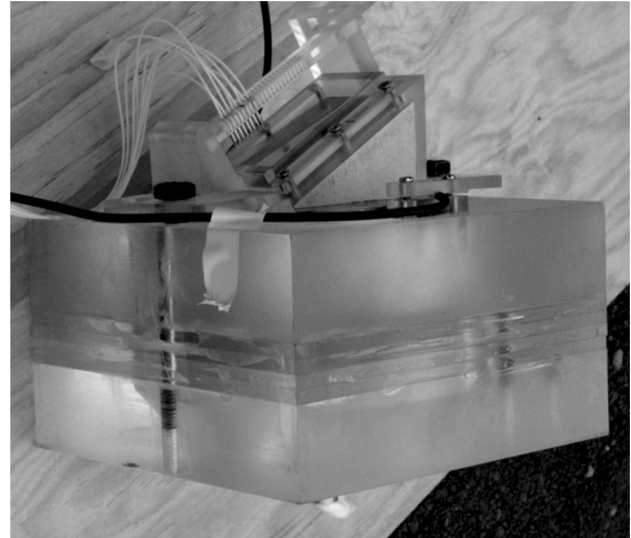


Figure 3. Photograph of the shock initiation experiment apparatus:

The apparent particle-velocity history $u(t)$ could be calculated according to the digitizer record and Equation (1) [8].

$$u(t) = \frac{\lambda F(t)}{2\tau} \cdot \frac{1}{1 + \delta} \quad (1)$$

where $F(t)$ is the frequency of the fringes, λ is the wavelength of the laser light, δ is a correction factor with respect to the wavelength for dispersion in the etalon (delay bar) material.

The measured quantities that determine the accuracy of this formula are the wavelength of the laser, the time base of the oscilloscope and the linearity of the detection. These three quantities have proven to be so ideal in practice that they do not limit the accuracy of the above analysis. The limitations are the noise fraction and width of the Fourier-transform window relative to the fringe period. As a result, velocity measurements with a photon Doppler velocimeter (PDV) are inherently simple and accurate, and have been

demonstrated to date to an accuracy of $\sim 0.1\%$. A typical accuracy is 1% at 1000 m/s, $\delta t < 5$ ns. In this study, data-reduction software converts the sinusoidal traces to a polar plot, then to a particle velocity as a function of time.

As discussed by Jensen [9], PDV diagnostics measure the apparent velocity, not the true velocity, when the laser light is transmitted through a window. Because the shockwave experiments require a window to maintain the stress during the experiment, it is necessary to determine window corrections so that the true velocity can be calculated from the measured apparent velocity by Equation (2).

$$u_p(t) = \frac{u(t) - \frac{d}{dt} \left[\int_{x_s(t)}^{x_s(t)} n(x', t) dx' \right]}{\cos \alpha} \quad (2)$$

where $u(t)$ is the apparent interface velocity, $u_p(t)$ is the true value, α is the angle of the wedge-shaped explosive sample, $n(x', t)$ is the refraction index profile in the window, $x(t)$ is the front face of the window material and $x_s(t)$ is the back face of the window material.

The fringes of the complete digitizer record for shock-initiation experiments oscillate about a center that shifts up and down at all time scales, and the amplitude varies similarly quickly. The particle velocities were calculated according to the experimental data and Equations (1) and (2).

3 Results and Discussion

3.1 Calculation of Impact Pressure

The shock-initiation properties of the unconfined wedge-shaped explosive sample were investigated at different input pressures, including 9.56 GPa, 8.57 GPa and 7.98 GPa. We used the same wedge-shaped explosive sample, window, rotating mirror streak camera and PDV in all the abovementioned experiments, which would enable the measurement errors consistent. The initial shock pressures of 9.56, 8.57, and 7.98 GPa were generated by a detonation device with a 6-, 8- and 10-mm-thick attenuator of tungsten alloy, respectively. The input particle velocity is an important variable to quantify the initiation process. According to the basic relationships of the shockwave, the initial particle velocity can be calculated from Equation (3).

$$u_p = \frac{p}{\rho_0 u_s} \quad (3)$$

where ρ_0 is the density of the explosive, u_s is the shockwave velocity, and u_p is the particle velocity.

Figure 4 shows the initial shock pressure profiles that were measured by the manganin piezoresistive pressure gauges that were placed between the sample and the attenuator. The input shockwave velocity was obtained by the rotating mirror streak camera. Table 1 lists the input shockwave velocity, the initial shock pressure that was

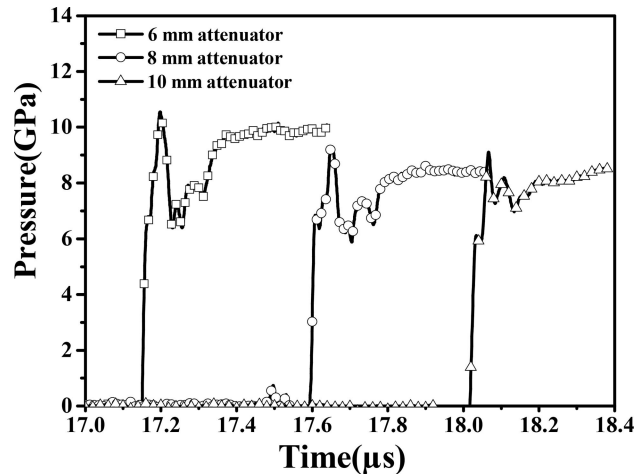


Figure 4. Manganin piezoresistive pressure gauge results for JBO-9021.

Table 1. Summary of the input shock characteristics.

Thickness of attenuator [mm]	Input pressure [GPa]	Input shock wave velocity [mm μs ⁻¹]	Input particle velocity [mm μs ⁻¹]
6	9.56	4.57	1.10
8	8.57	4.39	1.03
10	7.98	4.23	0.99

measured in the experiments and the input particle velocity that was calculated by using Equation (3). Here, the initial density of JBO-9021 was 1.905 g/cm³.

3.2 Particle Velocity and Shock Displacement vs. Time Waveforms

Three experiments were completed on JBO-9021 at several different initial shock pressures of 9.56, 8.57 and 7.98 GPa. Figure 5 shows that when the attenuator of the tungsten alloy was set to 6 mm, the measured pressure of the incident shockwave was 9.56 GPa. As the shockwave front propagated to a depth of 4, 5, 6, 7 and 8 mm into the sample surface, the particle velocities at these positions reached 1.15, 1.23, 1.38, 1.57 and 1.84 mm/μs, respectively. The slight particle-velocity increase behind the shock front at 4–8 mm suggests an incomplete reaction of the explosive and the absence of stable detonation. In comparison, the wavefront particle velocities at 6, 7 and 8 mm were 1.38, 1.57 and 1.84 mm/μs, respectively, which exceeded significantly the levels found at the same positions at shots 2 and 3. At 9 mm, the particle velocity reached 2.58 mm/μs at the wavefront and declined rapidly afterwards, which signaled that a stable detonation was obtained between 8 mm and 9 mm.

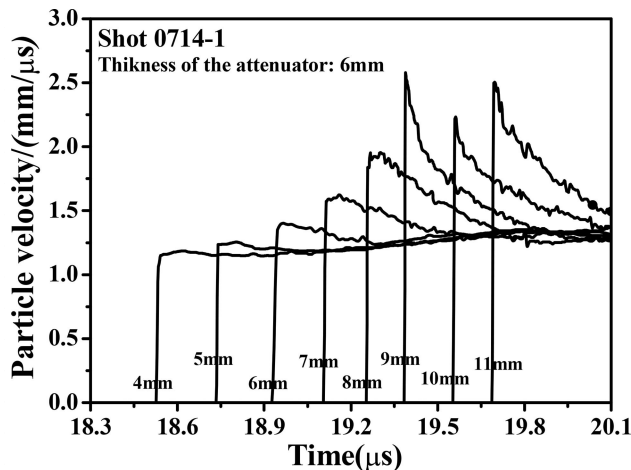


Figure 5. Particle velocity wave profiles from JBO-9021 experiment with a 9.56 GPa input.

Figure 6 shows particle-velocity wave profiles from the JBO-9021 experiment with a 8.57 GPa input. All wave profiles other than the last four showed that the amplitude of the wave at the shock front increases as the wave traveled into the sample. Compared with the wave profiles for an input pressure of 9.56 GPa, the rate of decline was gentler. The slight particle-velocity increase behind the shock front at 6–9 mm suggested an incomplete reaction of the explosive and the absence of stable detonation. The cyan wave profile was from the fiber probe that was located at a depth of 10 mm. According to this waveform, the particle velocity reached 2.65 mm/μs at the wavefront and declined rapidly afterwards, which signaled that a stable detonation was obtained between 9 mm and 10 mm.

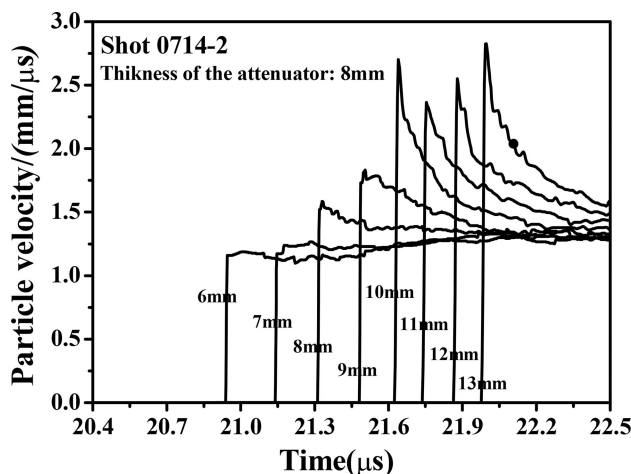


Figure 6. Particle velocity wave profiles from JBO-9021 experiment with a 8.57 GPa input.

The particle-velocity wave profiles from the JBO-9021 experiment with a 7.98 GPa input are shown in Figure 7. When the wave reached the first fiber probe, which was located at a depth of 4 mm, the particle velocity increased to 1.00 mm/μs and grew slightly to 1.15 mm/μs. This showed that the energy that was released during the decomposition reaction of the explosive had supported the shock-wave propagation already, and a turnover to detonation occurred at a depth of approximately 11 mm. The seven wave profiles from the fiber probes at depths of 4 through 10 mm showed a process of shock leading to detonation.

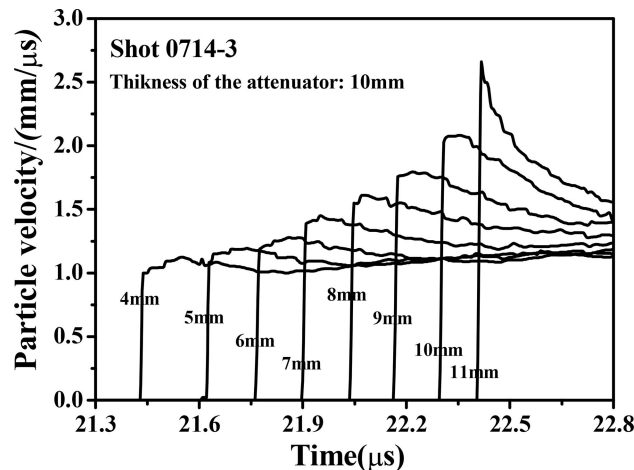


Figure 7. Particle velocity wave profiles from JBO-9021 experiment with a 7.98 GPa input.

As shown in Figure 5–7, the wavefront particle velocities measured at 6, 7 and 8 mm increased from 8.57 GPa to 9.56 GPa. The particle-velocity history profiles obtained at these experimental pressures showed an increasingly early manifestation of stable detonation. At 7.98 GPa, the peak particle velocity of the shock front was first observed at 11 mm, which indicated a run distance to detonation of 10–11 mm. In comparison, the explosive test sample achieved a stable detonation of ~10 mm at 8.57 GPa and ~9 mm at 9.56 GPa. We concluded that the propagation of the detonation wave was much faster at a 9.56 GPa input than at 7.98 GPa and 8.57 GPa.

The streak camera recorded the distance (x) and time (t) for the shock-initiation experiments in Figure 8, from which the data could be plotted as the inverse of the shockwave velocity (u_s) versus time (t). This presentation of data revealed the distance to detonation and initial shock velocity, and the results agreed well with the particle-velocity wave profiles from the JBO-9021 experiment with different inputs.

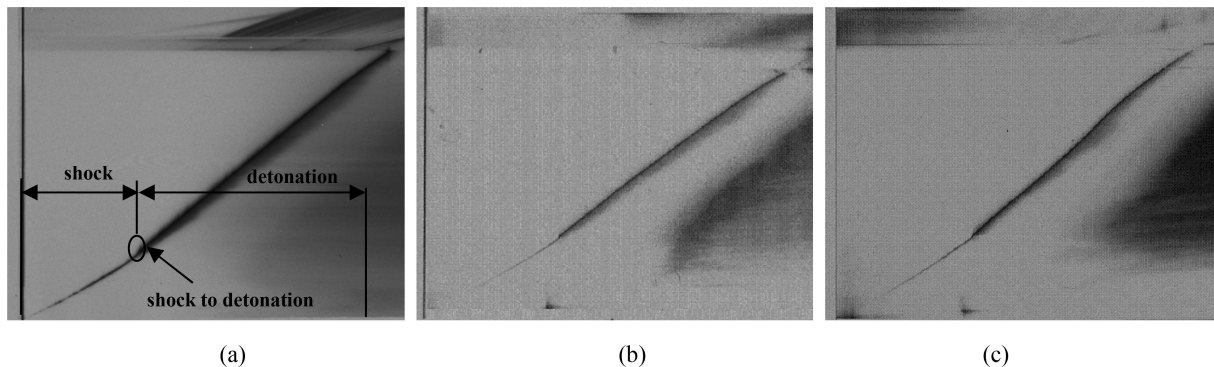


Figure 8. Shock wave profiles from JBO-9021 experiment at different initial shock pressure. (a) 9.56 GPa, (b) 8.57 GPa, (c) 7.98 GPa.

3.3 JBO-9021 Hugoniot

In the shock-initiation experiments, the particle-velocity profiles showed the following characteristics: the wavefront particle velocity that was induced only by the input shockwave and the energy release during the decomposition reaction did not affect the wavefront particle velocity. The wavefront particle velocity obtained by every fiber probe was induced only by the input shockwave, and the shockwave front is equivalent to an initial shock in the shock propagation. It could be assumed that these data met the shock Hugoniot relationship of an unreacted explosive. The unreacted Hugoniot can be explained by a linear relationship between the shockwave velocity u_s and the particle velocity u_p :

$$u_s = C + \lambda u_p \quad (4)$$

where C and λ are undetermined coefficients.

The results from the experiments, including the particle-velocity profiles measured by the PDV and the shock velocity measured by the rotating mirror streak camera, can be used to calculate the shock pressure p . These data are listed in Table 2. Figure 9 shows the u_s-u_p Hugoniot data for JBO-9021; a linear Rankine-Hugoniot fit to these data in the u_s-u_p plane is:

$$u_s = (1.352 \pm 0.300) + (2.933 \pm 0.222)u_p \quad (5)$$

3.4 Numerical Simulation

The explosive shock-initiation simulation model was established based on the shock-initiation experimental apparatus. The size of the simulation model was the same as the experimental apparatus. According to the symmetry of the device, a two-dimensional axisymmetric model was used. A numerical simulation was taken for the process of shock ini-

Table 2. Summary of JBO-9021 Hugoniot data, shock pressure and specific volume at shock front.

Shock wave velocity [mm μ s $^{-1}$]	Particle velocity [mm μ s $^{-1}$]	Pressure [GPa]
1.1	4.57	9.56
1.15	4.36	9.33
1.23	4.68	10.97
1.38	5.51	14.49
1.57	6.41	19.17
1.84	6.74	25.10
1.03	4.39	8.57
1.16	4.44	9.81
1.17	5.07	11.30
1.52	5.85	16.94
1.75	6.33	21.77
0.99	4.23	7.98
1	4.47	8.32
1.11	4.52	9.56
1.18	5.26	11.82
1.38	5.41	14.22
1.55	5.52	16.30
1.76	6.59	23.44

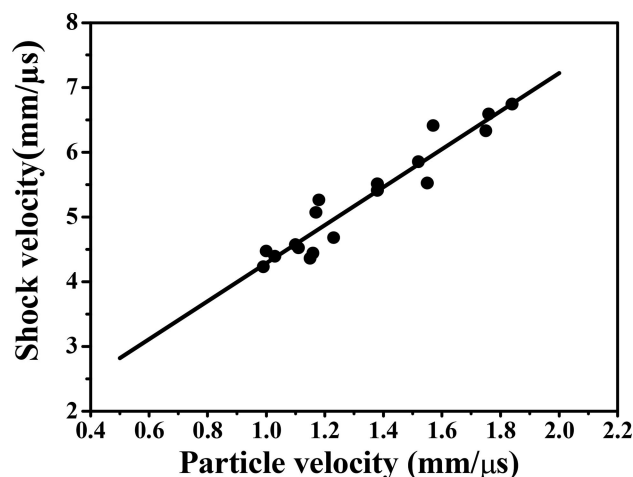


Figure 9. Fitted curve of u_s-u_p (Hugoniot relation of JBO-9021).

Table 3. Parameters for TNT and JO-9159 explosive.

Explosive	A [GPa]	B [GPa]	R ₁	R ₂	ω	E ₀ [GJ m ⁻³]	ρ ₀ [g cm ⁻³]	P _{CJ} [GPa]	D [cm μs ⁻¹]
TNT	371.3	3.23	4.15	0.95	0.30	7.0	1.64	27.0	0.6930
JO-9159	880.7	18.36	4.62	1.32	0.38	10.4	1.84	34.4	0.8700

tiation to detonation with the nonlinear finite-element method LS-DYNA.

A high-explosive burn model and equation of state in Jones-Wilkins-Lee (JWL) form were used to model TNT and JO-9159 (a HMX-based explosive), which were in the explosive plane wave lens and booster explosive. The parameters for TNT and JO-9159 are shown in Table 3. ρ₀ is the initial density, D is detonation velocity and P_{CJ} is the shock pressure at the CJ state.

In the numerical simulation, the tungsten-alloy attenuator and LiF single crystal were described by an elastic-plastic hydromaterial model and equation of state in the Gremisen form. The Gremisen equation of state with a cubic shock velocity-particle velocity defines the pressure for compressed materials as:

$$P = \frac{\rho_0 C^2 \mu (1 + (1 - \frac{\gamma_0}{2})\mu - \frac{a}{2}\mu^2)}{1 - (S_1 - 1)\mu - S_2 \frac{\mu^2}{\mu+1} - S_3 \frac{\mu^3}{(\mu+1)^2}} + (\gamma_0 + a\mu)E \quad (6)$$

where C is the intercept of the u_s-u_p curve; S₁, S₂ and S₃ are the coefficients of the slope of the u_s-u_p curve; γ₀ is the Gremisen gamma; a is the first-order volume correction to γ₀ and μ = ρ/ρ₀ - 1. The Gremisen parameters for the inert materials are listed in Table 4.

Table 4. Gremisen parameters for inert materials.

inert materials	ρ ₀ [g cm ⁻³]	C [mm μs ⁻¹]	S ₁	S ₂	S ₃	γ ₀	a
Tungsten alloy	19.2	4.03E+03	1.24	0.00	0.00	1.54	0.00
LiF single crystal	2.64	5.148E+03	1.358	0.00	0.00	1.69	0.00

An ignition and growth reactive-flow model was used to simulate the shock initiation of the JBO-9021 explosive. A JWL equation of state is used in this reactive-flow model for the unreacted explosive and the reaction products; the equation of state has the form:

$$P = Ae^{-R_1 v} + Be^{-R_2 v} + \frac{\omega C_v T_0}{v} \quad (7)$$

where v is the relative volume; T₀ is the initial temperature; P is the reaction product pressure; C_v is the heat capacity of the reaction products or unreacted HE and A, B, R₁, R₂ and w are adjustable constants.

The chemical reaction rate for the conversion of unreacted explosive to reaction products is:

$$\frac{d\lambda}{dt} = I(1 - \lambda)^b (\rho/\rho_0 - 1 - a)^x + G_1(1 - \lambda)^c \lambda^d p^y + G_2(1 - \lambda)^e \lambda^f p^z \quad (8)$$

where λ is the fraction reacted; t is time; ρ is the current density; ρ₀ is the initial density; P is pressure and I, G₁, G₂, a, b, c, d, e, f, x, y and z are adjustable constants.

The unreacted JWL equation of state parameter was determined from the Rankine-Hugoniot relationships. The product JWL EOS parameters were obtained from the cylinder test for the JBO-9021 explosive. The particle-velocity waveforms measured in the experiments provide valuable data to calibrate the ignition and growth reactive-flow model. The EOS parameters and ignition and growth reactive-flow model parameters are shown in Table 5.

Table 5. Ignition and growth model parameters for JBO-9021.

Unreacted JWL	Product JWL	Reaction rate parameters	
A = 778.1 GPa	A = 449.0 GPa	I = 4.0 × 10 ⁶	G ₂ = 30
B = -5.031 GPa	B = 13.39 GPa	a = 0.02	e = 0.667
R ₁ = 11.31	R ₁ = 3.852	b = 0.667	f = 0.667
R ₂ = 1.130	R ₂ = 1.031	x = 7.0	z = 1.0
w = 0.8835	w = 0.4601	G ₁ = 9000	Figmatx = 0.01
C _v = 2.491 × 10 ⁻⁵ Gpa K ⁻¹	C _v = 1.012 × 10 ⁻⁵ Gpa K ⁻¹	c = 0.667	FG1max = 0.8
T ₀ = 298 K	T ₀ = 298 K	d = 0.67	FG2 min = 0.8
ρ ₀ = 1.905 g cm ⁻³	ρ ₀ = 1.905 g cm ⁻³	y = 3.0	

Figure 10 compares the measured and calculated particle-velocity histories for shock initiation on JBO-9021 at 9.56 GPa. The PDV record and calculated particle-velocity profiles almost overlap at every portion of the data. The calculated results are consistent with the evolution of shock into a detonation, which indicates that these JWL EOS and ignition and growth reactive-flow model parameters can describe the shock initiation characteristics of JBO-9021.

The distance to detonation as a function of initial shock pressure, the Pop-plot, can reflect the shock sensitivity of the explosive to some extent. Hence, a shock-initiation simulation model was established to calculate the Pop-plot. This model was composed of a booster explosive, tungsten-alloy attenuator and explosive sample. The details are shown in Figure 11. A plane shockwave is generated by the

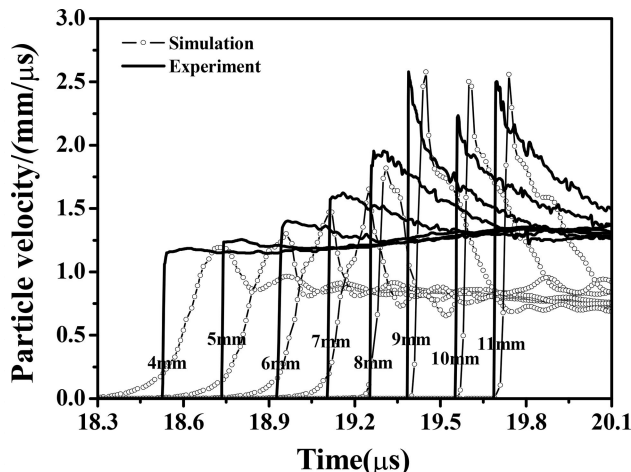


Figure 10. Experimental and calculated particle velocity profiles in shock initiation of JBO-9021 at 9.56 GPa pressure.

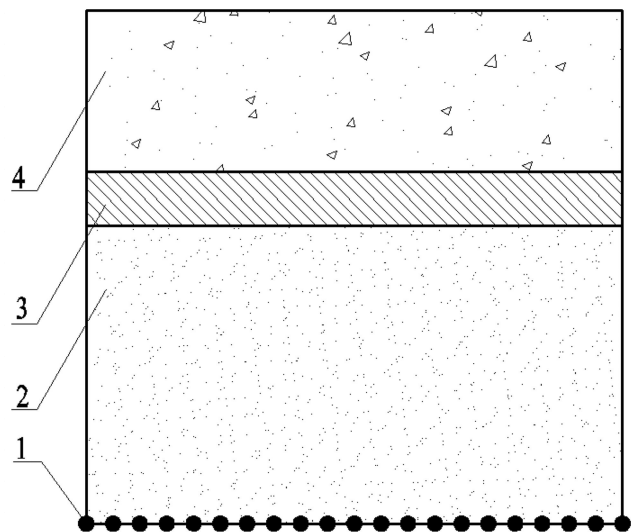


Figure 11. Shock initiation simulation model. 1- Initial point, 2- Booster explosive, 3- Tungsten alloy attenuator, 4- Explosive specimen.

booster explosive with twenty initial points, and the initial shock pressure can be adjusted by changing the thickness of the tungsten-alloy attenuator. With this simulation model, the distance to detonation at different initial shock pressures can be calculated. The Greeneisen parameters for the tungsten-alloy is listed in Table 4. A high-explosive burn model and equation of state in JWL form were used to model the booster explosive (JO-9159). The JO-9159 parameters are shown in Table 3. The unreacted and product JWL EOS and ignition and growth reactive-flow model were used to model the explosive sample.

The experimental data points of distance to detonation at different initial shock pressures for JBO-9021, PBX9502 (TATB/ Kel-F/95/5) [10–11], LX-17 (TATB/ Kel-F/92.5/7.5) [11–

13], LX-10 (HMX/Viton/95/5) [14] and PBX 9501 (HMX/Binder/95/5) [15] are shown in Figure 12. The black line is the distance to a detonation versus an initial shock pressure of JBO-9021 that was obtained from the numerical simulation. This line shows only a predicted trend in the higher-pressure regime, which should be verified in further experiments. The shock sensitivity of JBO-9021 was observed to be slightly higher than that of LX-17 and PBX 9502, which comprise TATB primarily and is significantly lower than that of LX-10 and PBX 9501, which comprise HMX primarily. The shock sensitivity of JBO-9021 is among the most insensitive explosives.

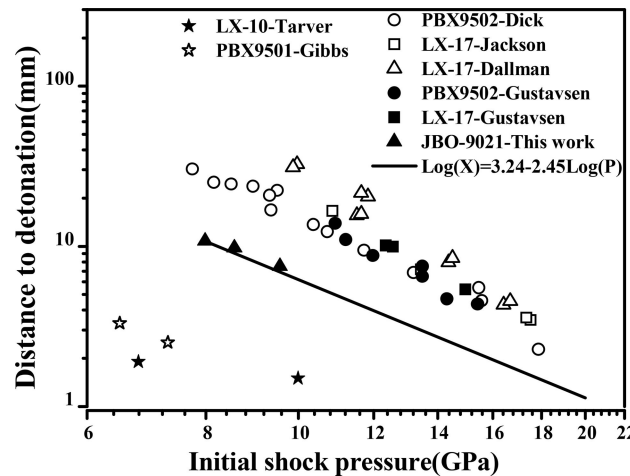


Figure 12. Pop-plot for JBO-9021, PBX9502, LX-17, LX-10 and PBX9501.

4 Conclusions

A multi-point laser interferometer, termed the photon Doppler velocimeter, and a rotating mirror streak camera were used to investigate the evolution of shock into detonation of a new insensitive high explosive termed JBO-9021. The explosion was used to yield experimental pressure-history curves that offered valuable insight into the shock-initiation properties of the JBO-9021 explosive samples under these conditions. By using the photon Doppler velocimeter and streak camera, the particle velocity at several distances from the impact surface and the shockwave velocities were measured. The evolution of the shock into a detonation of JBO-9021 explosive at several shock input pressures was investigated. Hugoniot data for JBO-9021 were obtained according to the increase in particle velocity in the unreacted sample.

The development of an ignition and growth reactive-flow model and its parameters calibrated by the particle-velocity profiles measured in the experiments allowed us to perform mathematical simulations for the detonation of the JBO-9021 explosive test sample at different input pressures. These coefficients were applied in the calculation of the

Pop-plot, and the shock sensitivity of the JBO-9021 is slightly higher than that of the LX-17 and PBX 9502 and tremendously lower than that of the LX-10 and PBX 9501.

References

- [1] K. S. Vandersall, C. M. Tarver, F. Garcia, P. A. Urtiew, S. K. Chidester, Shock Initiation Experiments on the HMX Based Explosives LX-07 and LX-10 with Associated Ignition and Growth Modeling, *14th American Physical Society Topical Conference on Shock Compression of Condensed Matter*, Kohala Coast, HI, USA, June 24–29, **2007**, 955.1, pp. 1010–1013.
- [2] L. M. Barker, R. E. Hollenbach, Laser Interferometer for Measuring High Velocities of Any Reflecting Surface, *J. Appl. Phys.* **1972**, 43, 4669–4675.
- [3] J. Wackerle, H. L. Stacy, W. L. Seitz, Velocimetry studies on the prompt initiation of PBX 9502, *10th Int. Symposium on Detonation*, Boston, MA, USA, July 12–16, **1993**.
- [4] W. M. Trott, *13th Int. Symposium on Detonation*, Norfolk, VA, USA, July 23–28, **2008**.
- [5] K. J. Fleming, *12th Int. Symposium on Detonation*, San Diego, CA, USA, August 11–16, **2002**, pp. 1097–1102.
- [6] M. E. Briggs, *14th Int. Symposium on Detonation*, Coeur D'Alene, ID, USA, April 11–16, **2010**.
- [7] E. Dudley, D. Damm, E. Welle, *14th Int. Symposium on Detonation*, Coeur D'Alene, ID, USA, April 11–16, **2010**.
- [8] L. M. Barker, K. W. Schuler, Correction to the velocity-per-fringe relationship for the VISAR interferometer, *J. Appl. Phys.* **1974**, 45, 3692–3693.
- [9] B. J. Jensen, D. B. Holtkamp, P. A. Rigg, D. H. Dolan, Accuracy limits and window corrections for photon Doppler velocimetry, *J. Appl. Phys.* **2007**, 101, 523–454.
- [10] J. J. Dick, C. A. Forest, The Hugoniot and shock sensitivity of a plastic-bonded TATB explosive PBX 9502, *J. Appl. Phys.* **1988**, 63, 4881–4888.
- [11] R. L. Gustavsen, S. A. Sheffield, R. R. Alcon, J. W. Forbes, C. M. Tarver, F. Garcia, Embedded Electromagnetic Gauge Measurements and Modeling of Shock Initiation in the TATB Based Explosives LX-17 and PBX 9502, CP620, Shock Compression of Condensed Matter – 2001, American Institute of Physics, **2002**, 1019–1022.
- [12] J. C. Dallman, Jerry Wackerle, *10th Int. Symposium on Detonation*, Boston, MA, USA, July 12–16, **1993**.
- [13] R. K. Jackson, *6th Int. Symposium on Detonation*, Coronado, CA, USA, August 24–27, **1976**.
- [14] C. M. Tarver, J. O. Hallquist, L. M. Erickson. Modeling short pulse duration shock initiation of solid explosives, *8th Intern. Symp. on Detonation*, Albuquerque, NM, USA, July 14–18, **1985**.
- [15] T. R. Gibbs, A. Popolato, J. F. Baytos. LASL explosive property data, University of California Press, **1980**.

Manuscript received: March 11, 2018

Revised manuscript received: June 26, 2018

Version of record online: November 29, 2018